Advances in Continuous and Discrete Models

RESEARCH Open Access

Computing confined elasticae

Sören Bartels[1*] and Pascal Weyer[1]

*Correspondence:
bartels@mathematik.uni-freiburg.de
[1]Abteilung für Angewandte Mathematik,
Albert-Ludwigs-Universität Freiburg,
Hermann-Herder-Str. 10, 79104
Freiburg i. Br., Germany

Abstract

We devise a numerical scheme for computing arc-length parameterized curves of low bending energy that are confined to convex domains. We address the convergence of the discrete formulations to a continuous model and the unconditional stability of an iterative scheme. Numerical simulations confirm the theoretical results and lead to a classification of observed optimal curves within spheres.

MSC: 65N30; 35Q74; 65N12; 74K10

Keywords: Rods; Elasticity; Constraints; Numerical scheme

1 Introduction

Equilibrium configurations of thin elastic rods have been of interest since the times of Euler. The mathematical modeling of these deformable structures has been reduced from three dimensions to a one-dimensional problem for the centerline of the rod $u : I \to \mathbb{R}^3$; see [8, 22, 29, 32, 37]. In the bending regime the rod is inextensible so that $|u'| = 1$ on I. Considering a circular cross section and omitting twist contributions, the elastic energy reduces to the functional

$$E_{\mathrm{bend}}[u] = \frac{\kappa}{2} \int_I \left|u''(x)\right|^2 \mathrm{d}x$$

for a parameter $\kappa > 0$ that describes the bending rigidity. Elasticae, i.e., rods of minimal bending energy, can be stated explicitly, e.g., for periodic boundary conditions [33, 34]. Applications of elastic thin rods include DNA modeling [1, 27, 43], the movement of actin filaments in cells [36] or of thin microswimmers [41], the fabrication of textiles [30], and investigating the reach of a rod injected into a cylinder [38].

To obtain minimally bent elastic rods, the bending energy can be reduced by a gradient-flow approach. This method can be used for analytic considerations, cf. for instance [19, 26, 34, 39, 42] and numerical computations [2–7, 13–15, 20, 21, 25, 45]. An efficient finite-element approach with an accurate treatment of the inextensibility condition can be used to find equilibria of free elastic rods [7] and self-avoiding rods [12, 13]. It can also be generalized to include twist contributions defined via torsion quantities [11]. We follow common conventions and refer to rods as *elastic curves* when twist contributions are omitted.

© The Author(s) 2022. **Open Access** This article is licensed under a Creative Commons Attribution 4.0 International License, which permits use, sharing, adaptation, distribution and reproduction in any medium or format, as long as you give appropriate credit to the original author(s) and the source, provide a link to the Creative Commons licence, and indicate if changes were made. The images or other third party material in this article are included in the article's Creative Commons licence, unless indicated otherwise in a credit line to the material. If material is not included in the article's Creative Commons licence and your intended use is not permitted by statutory regulation or exceeds the permitted use, you will need to obtain permission directly from the copyright holder. To view a copy of this licence, visit http://creativecommons.org/licenses/by/4.0/.

In this paper, we prpose a generalization of the existing scheme [7] to calculate elasticae of *confined* elastic curves. Confinements of elastic structures arise on a variety of length scales, such as DNA plasmids or biopolymers inside a cell or chamber [18, 40]. The boundary of closely packed elastic sheets or a wire in a container can be modeled as confined elastic rods in two dimensions [16, 23]. Planar settings have been addressed numerically and analytically in [24, 46], and a numerical scheme for thick elastic curves in containers is devised in [44].

We propose an approach that can be used for rods embedded in arbitrary dimensions confined to convex domains. For the mathematical modelling, we use a gradient flow to minimize the bending energy. The admissible rod configurations during the flow are restricted to a domain $D \subset \mathbb{R}^3$.

The task to unbend a rod inside D can be translated to minimizing E_{bend} among all

$$u \in \mathcal{A}_D = \left\{ v \in H^2\left(I;\mathbb{R}^3\right) : v \in D \text{ and } \left|v'\right| = 1 \text{ a.e., } L_{\mathrm{bc}}(v) = \ell_{\mathrm{bc}} \right\}.$$

Since the constraint $v(x) \in D$ will be treated via a penalty approach, we also make use of the set of unconstrained curves

$$\mathcal{A} = \left\{ v \in H^2\left(I;\mathbb{R}^3\right) : \left|v'\right| = 1 \text{ a.e., } L_{\mathrm{bc}}(v) = \ell_{\mathrm{bc}} \right\}.$$

The bounded linear operator $L_{\mathrm{bc}} : H^2(I;\mathbb{R}^3) \to \mathbb{R}^\ell$ realizes appropriate boundary conditions, e.g., periodic boundary conditions are imposed via $L_{\mathrm{bc}}(v) = 0$ with

$$L_{\mathrm{bc}}(v) = \left(v(b) - v(a), v'(b) - v'(a)\right)$$

if $I = (a, b)$. Since we aim at the construction of an efficient numerical scheme, we restrict our considerations to those subsets D that can be written as finite intersections of *simple quadratic confinements* D_r, $r = 1, 2, \ldots, r_D$, i.e.,

$$D = \bigcap_{r=1}^{r_D} D_r, \quad D_r = \left\{ y \in \mathbb{R}^3 : |y|_{D_r}^2 = y \cdot G_{D_r} y \le 1 \right\}$$

for symmetric positive semidefinite matrices $G_{D_r} \in \mathbb{R}^{3\times 3}$. We call the finite intersection a *composite quadratic confinement*. Our scheme therefore excludes the sets defined by, e.g., other vector norms, such as $D = \{y \in \mathbb{R}^3 : |y|_p^2 \le 1\}$ with $p \neq 2$. For ease of presentation, we often consider one set D_r and then omit the index r. Some basic simple quadratic confinements are the ball with radius R and $G_D = I_3/R^2$, the ellipsoid with radii R_1, R_2, R_3 and $(G_D)_{ij} = \delta_{ij}/R_i^2$, or the space between two parallel planes with distance $2R$ with normal vector n and $G_D = nn^t/R^2$. Infinite cylinders have $(G_D)_{ii} = 0$ for exactly one index i. Boxes and finite cylinders can be constructed as composite quadratic confinements. In general, any simple or composite quadratic confinement is a convex, closed, and connected set. We remark that our convergence analysis also applies to nonquadratic confinements, but the efficiency of the devised iterative scheme substantially depends on this feature.

We enforce the confinement via a potential approach, so a nonnegative term is added to the bending energy whenever the curve violates the confining restrictions. We define

the potential $V_D : \mathbb{R}^3 \to \mathbb{R}$ for a simple quadratic confinement D that vanishes in D and is strictly positive on $\mathbb{R}^3 \backslash D$ via

$$V_D(y) = \frac{1}{2}\big(|y|_D - 1\big)_+^2 = \frac{1}{2}|y|_D^2 + \frac{1}{2}V_D^{\mathrm{cv}}(y),$$

where the concave part V_D^{cv} is given by the continuous function

$$V_D^{\mathrm{cv}}(y) = \begin{cases} -|y|_D^2 & \text{if } y \in D, \\ -2|y|_D + 1 & \text{otherwise.} \end{cases}$$

The potential is used to define the penalizing *confinement energy* functional

$$E_D[u] = \int_I \big|u(x)\big|_D^2 + V_D^{\mathrm{cv}}\big(u(x)\big)\,\mathrm{d}x,$$

which is nonnegative by the definition of the potential and zero if and only if the curve entirely lies within D. For a composite confinement defined via a family $(D_r)_{r=1,\dots,r_D}$ of simple quadratic confinements, we sum the corresponding confinement energies up, i.e.,

$$E_D[u] = \sum_{r=1}^{r_D} E_{D_r}[u], \qquad V_D(y) = \sum_{r=1}^{r_D} V_{D_r}(y). \tag{1}$$

We remark that translated domains and half-spaces, e.g., $D = \{y \in \mathbb{R}^3 : |y - y_D|_D^2 \le 1\}$ and $D = \{y \in \mathbb{R}^3 : a_D \cdot y \le 1\}$, can be similarly treated.

Given $\varepsilon > 0$, a curve $u_\varepsilon \in \mathcal{A}$ is called an (*approximately*) *confined elastica* if it is stationary for the functional

$$E_\varepsilon[u] = E_{\mathrm{bend}}[u] + \frac{1}{2\varepsilon}E_D[u]$$

in the set $\mathcal{A}$. If $V_D(u_\varepsilon) = 0$ almost everywhere on I, then the rod is called an *exactly confined elastica.* The parameter ε determines the steepness of the quadratic well potential and defines a length-scale for the penetration depth of the curve into the space outside of D.

Considering a simple quadratic confinement $D \subset \mathbb{R}^3$, we let $V_D \in C^1(\mathbb{R}^3;\mathbb{R})$ be the corresponding quadratic-well potential and choose $\varepsilon > 0$. Trajectories $u \in H^1([0,T];L^2(I;\mathbb{R}^3)) \cap L^\infty([0,T];\mathcal{A})$ are defined by gradient flow evolutions. In particular, for an inner product $(\cdot,\cdot)_\star$ on $L^2(I;\mathbb{R}^3)$ and an initial configuration $u(0,x) = u_0(x)$, we define the temporal evolution as the solution of the time-dependent nonlinear system of partial differential equations

$$\begin{aligned} &(\partial_t u, v)_\star + \kappa\big(u'', v''\big) + \varepsilon^{-1}(u, G_D v) \\ &\quad = -(2\varepsilon)^{-1}\big(\nabla V_D^{\mathrm{cv}}(u), v\big) - \big(\lambda u', v'\big) \end{aligned} \tag{2}$$

for test functions $v \in \mathcal{V}$ with a suitable set $\mathcal{V}$ and all $t \in [0,T]$. The function $\lambda \in L^1([0,T] \times I)$ is a Lagrange multiplier associated with the arc-length condition. Confined elasticae are stationary points for (2).

For time discretization, we use backward differential quotients. Let $\tau > 0$ be the fixed time-step, and let $k \geq 0$ be a nonnegative integer. We set $u^0 := u_0$ and define the time step

$$d_t u^{k+1} = \frac{u^{k+1} - u^k}{\tau}.$$

The gradient flow system is evaluated implicitly except for the concave confinement energy, which is handled explicitly due to its nonlinearity and antimonotonicity, and the Lagrange multiplier term, which is treated semiimplicitly. We hence have

$$\begin{aligned} &\big(d_t u^{k+1}, v\big)_\star + \kappa\big(\big[u^{k+1}\big]'', v''\big) + \varepsilon^{-1}\big(u^{k+1}, G_D v\big) \\ &\quad = -(2\varepsilon)^{-1}\big(\nabla V_D^{\mathrm{cv}}\big(u^k\big), v\big) - \big(\lambda^{k+1}\big[u^k\big]', v'\big) \end{aligned} \tag{3}$$

for suitable test curves $v \in \mathcal{V}$. To ensure that the parameterization by arc-length is approximately preserved throughout the gradient flow, the constraint $|[u^k]'|^2 = 1$ is linearized. This yields the first-order orthogonality condition

$$\big[u^k\big]' \cdot \big[d_t u^{k+1}\big]' = 0 \quad \text{on } I. \tag{4}$$

By imposing the same condition on test curves, i.e.,

$$\big[u^k\big]' \cdot v' = 0 \quad \text{on } I, \tag{5}$$

the Lagrange multiplier term disappears in (4). Given $u^0, u^1, \dots, u^k \in H^2(I;\mathbb{R}^3)$, there are unique functions $d_t u^{k+1} \in H^2(I;\mathbb{R}^3)$ that solve the gradient flow equation (3) with all v satisfying (5) and $L_{\mathrm{bc}}[v] = 0$. This is a direct consequence of the Lax–Milgram lemma, provided that $v \mapsto \|v\|_\star + \|v''\|$ defines an equivalent norm on the kernel of L_{bc} as a closed subspace of $H^2(I;\mathbb{R}^3)$.

For numerical computations, we subdivide I into a partition $\mathcal{P}_h$ of maximal length h, which can be represented by the nodes $x_0 < x_1 < \cdots < x_N$. We use the space of piecewise cubic, globally continuously differentiable splines on $\mathcal{P}_h$ as a conforming subspace $V_h \subset H^2(I)$. On an interval $[x_i, x_{i+1}]$, these functions are entirely defined by the values and the derivatives at the endpoints. We also employ the space of piecewise linear, globally continuous finite element functions determined by the nodal values and denote the set by W_h. The corresponding interpolation operators are denoted as $\mathcal{I}_{3,h}$ and $\mathcal{I}_{1,h}$, respectively. We impose the orthogonality of $d_t u_h^{k+1}$ and u_h^k only at the nodes. The confinement quantities are evaluated by mass lumping, so only the values

$$(v, w)_h := \int_I \mathcal{I}_{1,h}(v \cdot w)\,\mathrm{d}x$$

at the nodes are required. In the nodal points the concavity of V_D^{cv} is used to prove an energy monotonicity property.

We consider a controlled violation of the arclength constraint at the nodes of the partitioning determined by a parameter $\delta_h \geq 0$ and define the discrete admissible set via

$$\mathcal{A}_h := \big\{u_h \in V_h^3 : \big|\big|u_h'(x_i)\big|^2 - 1\big| \leq \delta_h,\ i = 0, 1, \dots, N,\ L_{\mathrm{bc}}[u_h] = \ell_{\mathrm{bc}}\big\}.$$

The set of test functions relative to u_h is

$$\mathcal{F}_h[u_h] := \{v_h \in V_h^3 : u_h'(x_i) \cdot v_h'(x_i) = 0,\ i = 0, 1, \dots, N,\ L_{\mathrm{bc}}[v_h] = 0\}.$$

We thus obtain the following fully practical numerical scheme to compute confined elasticae: Given $u_h^0 \in \mathcal{A}_h$, define $u_h^1, \dots, u_h^k \in V_h^3$ by calculating $d_t u_h^{k+1} \in \mathcal{F}_h[u_h^k]$ such that

$$\begin{aligned}&\big(d_t u_h^{k+1}, v_h\big)_\star + \kappa\big(\big[u_h^k\big]'' + \tau\big[d_t u_h^{k+1}\big]'', v_h''\big) + \varepsilon^{-1}\big(u_h^k + \tau d_t u_h^{k+1}, G_D v_h\big)_h \\ &\quad = -(2\varepsilon)^{-1}\big(\nabla V_D^{\mathrm{cv}}\big(u_h^k\big), v_h\big)_h\end{aligned} \tag{6}$$

for all $v_h \in \mathcal{F}_h[u_h^k]$.

The key feature of our numerical method is that it detects stationary configurations of low energy. It can in general not be guaranteed that these are global minimizers, but the stable symmetries observed in the experiments for different starting values indicate that this is often the case. Our convergence theory assumes almost global discrete minimizers. Different approaches based on working with the Euler–Lagrange equations or using additional properties of the energy functional can lead to more general convergence theories but are beyond the scope of our paper.

The remainder of the paper is structured into a first part proving the convergence of the proposed numerical scheme and into a second part that presenting the results of numerical experiments and describes confined elasticae for closed rods in balls. The numerical simulations were done in the web application Knotevolve [9], which is accessible at aam.uni-freiburg.de/knotevolve.

2 Convergence results

In this section, we provide convergence results following ideas from [10]. The first result establishes the unconditional variational convergence of the discrete minimization problems to the continuous one defining confined elasticae. The following partial Γ convergence result relies on a regularity condition and is a consequence of conformity properties of the discrete model. We assume the setting introduced above, in particular, that $L_{\mathrm{bc}} : H^2(I;\mathbb{R}^3) \to \mathbb{R}^\ell$ is a bounded linear operator depending on the boundary values of a function and its derivatives and that $D \subset \mathbb{R}^3$ is convex and closed.

Proposition 1 *Define* $E_h : H^2(I;\mathbb{R}^3) \to \mathbb{R} \cup \{+\infty\}$ *via*

$$E_{h,\varepsilon}[u_h] = \frac{\kappa}{2}\int_I \big|u_h''\big|^2\,\mathrm{d}x + \frac{1}{2\varepsilon}\int_I \mathcal{I}_{1,h} V_D(u_h)\,\mathrm{d}x$$

if $u_h \in \mathcal{A}_h$ *and* $E_h[u_h] = +\infty$ *if* $u_h \in H^2(I;\mathbb{R}^3) \setminus \mathcal{A}_h$. *Analogously, let*

$$E_{\mathrm{bend}}[u] = \frac{\kappa}{2}\int_I \big|u''\big|^2\,\mathrm{d}x$$

for $u \in \mathcal{A}_D$ *and* $E_{\mathrm{bend}}[u] = +\infty$ *if* $u \in H^2(I;\mathbb{R}^3) \setminus \mathcal{A}_D$.

(i) *For every sequence* $(u_h)_{h>0} \subset H^2(I;\mathbb{R}^3)$ *with weak limit* $u \in H^2(I;\mathbb{R}^3)$, *we have* $E_{\mathrm{bend}}[u] \le \liminf_{(h,\varepsilon)\to 0} E_{h,\varepsilon}[u_h]$.

(ii) *For every* $u \in \mathcal{A}_D$ *with* $u \in H^3(I;\mathbb{R}^3)$, *there exists a sequence* $(u_h)_{h>0} \subset H^2(I;\mathbb{R}^3)$ *such that* $\lim_{(h,\varepsilon)\to 0} E_{h,\varepsilon}[u_h] = E_{\mathrm{bend}}[u]$.

Proof Throughout this proof, we write $h \to 0$ for a sequence $(h,\varepsilon) \to 0$.

(i) We consider a sequence $(u_h)_{h>0} \subset H^2(I;\mathbb{R}^3)$ and a limit $u \in H^2(I;\mathbb{R}^3)$ with $u_h \rightharpoonup u$ in $H^2(I;\mathbb{R}^3)$ as $h \to 0$. The compact embedding of H^2 into L^2 allows us to assume (after extraction of a subsequence) that $u_h \to u$ strongly in $L^2(I;\mathbb{R}^3)$. To show that $E[u] \le \liminf_{h\to 0} E_{h,\varepsilon}[u_h]$, it suffices to consider the case that the limit inferior is finite. Since $|\mathcal{I}_{1,h}|u_h'|^2 - 1| \le \delta_h$, we find that

$$\begin{aligned}\big\|\,|u_h'|^2 - 1\big\|_{L^2(I)} &\le \big\|\,|u_h'|^2 - \mathcal{I}_{1,h}|u_h'|^2\big\|_{L^2(I)} + \big\|\mathcal{I}_{1,h}|u_h'|^2 - 1\big\|_{L^2(I)}\\ &\le ch\big\|\big(|u_h'|^2\big)'\big\|_{L^2(I)} + c\delta_h\\ &\le ch\big\|u_h''\big\|_{L^2(I)}\big\|u_h'\big\|_{L^\infty(I)} + c\delta_h,\end{aligned}$$

which implies that $|u'|^2 = 1$ in I. Similarly, since $\|\mathcal{I}_{1,h}V_D(u_h)\|_{L^1(I)} \to 0$, it follows that $u \in D$ in I. Since the bending energy is weakly lower semicontinuous and the potential term is nonnegative, we deduce the stated inequality.

(ii) Given $u \in \mathcal{A}_D$ such that $u \in H^3(I;\mathbb{R}^3)$, we define $u_h = \mathcal{I}_{3,h}u$ and note that $u_h \to u$ in $H^2(I;\mathbb{R}^3)$ and $u_h(x_i) \in D$ as well as $|u_h'(x_i)| = 1$ for all $i = 0,1,\dots,N$, in particular, $u_h \in \mathcal{A}_h$. This implies that $\lim_{h\to 0} E_{h,\varepsilon}[u_h] = E_{\mathrm{bend}}[u]$. □

Remark 2 The regularity condition can be avoided if a density result for inextensible confined curves in the spirit of [31] is available. Alternatively, a standard regularization of a given curve $u \in \mathcal{A}_D$ can be considered following [11, 14], which requires an appropriate scaling of the discretization and penalty parameters.

The proposition implies the convergence of discrete (almost) minimizers, provided that the boundary conditions imply a coercivity property and exact minimizers are regular. We say that $u_h \in \mathcal{A}_h$ is a *discrete almost minimizer* if $E_{h,\varepsilon}[u_h] \le \min_{v_h\in\mathcal{A}_h} E_{h,\varepsilon}[v_h] + \varrho_h$ with tolerance $\varrho_h \ge 0$ satisfying $\varrho_h \to 0$ as $h \to 0$.

Corollary 3 *Assume that minimizers* $u \in \mathcal{A}_D$ *for* E_{bend} *satisfy* $u \in H^3(I;\mathbb{R}^3)$ *and that there exists* $c > 0$ *such that* $\|v\|_{H^2(I)} \le c\|v''\|_{L^2(I)}$ *for all* $v \in H^2(I;\mathbb{R}^3)$ *with* $L_{\mathrm{bc}}[v] = 0$ *or* D *is bounded. Then sequences of discrete almost minimizers for* $E_{h,\varepsilon}$ *accumulate weakly in* $H^2(I;\mathbb{R}^3)$ *at minimizers for* E_{bend}.

Proof The assumed inequality implies that discrete almost minimizers $u_h = u_{\mathrm{bc},h} + u_{0,h}$ are bounded in $H^2(I;\mathbb{R}^3)$, where $(u_{\mathrm{bc},h})_{h>0}$ is a bounded sequence of discrete functions that satisfies $L_{\mathrm{bc}}(u_{\mathrm{bc},h}) = \ell_{\mathrm{bc}}$. Given a weak accumulation point $u \in H^2(I;\mathbb{R}^3)$ of the sequence $(u_h)_{h>0}$ with $u_h \in \mathcal{A}_h$ for all $h > 0$ and a minimizer $\widetilde{u} \in H^3(I;\mathbb{R}^3)$ for E, we choose a sequence $\widetilde{u}_h$ as in Proposition 1(ii). We then have that

$$E[u] \le \liminf_{h\to 0} E_{h,\varepsilon}[u_h] \le \liminf_{h\to 0} E_{h,\varepsilon}[\widetilde{u}_h] + \varrho_h = E[\widetilde{u}].$$

Hence $u \in \mathcal{A}_D$ is minimal for E. □

Our second convergence result concerns an estimate on the confinement violation.

Proposition 4 *Let $u_h \in \mathcal{A}_h$. Then*

$$\big\|\mathcal{I}_{1,h}\big(|u_h|_D - 1\big)_+\big\|_{L^\infty(I)} \le c\varepsilon^{1/3}\big(E_{h,\varepsilon}[u_h]\big)^{1/3}.$$

Proof The Gagliardo–Nirenberg inequality bounds the norm in $L^p(I)$ by the product of norms in $L^q(I)$ and $W^{1,r}(I)$ with exponents $1-\alpha$ and α such that $\frac{1}{p} + \frac{1}{q} = \alpha(1 - \frac{1}{r} + \frac{1}{q})$; see [35]. With $p = r = \infty$, $q = 2$, and $\alpha = 1/3$, we have

$$\big\|\mathcal{I}_{1,h}\big(|u_h|_D - 1\big)_+\big\|_{L^\infty(I)} \le c\big\|\mathcal{I}_{1,h}\big(|u_h|_D - 1\big)_+\big\|_{L^2(I)}^{2/3}\big\|\mathcal{I}_{1,h}\big(|u_h|_D - 1\big)_+\big\|_{W^{1,\infty}(I)}^{1/3}.$$

The $W^{1,\infty}$ norm can be uniformly bounded due to the stability of the nodal interpolation operator in $W^{1,\infty}$ and the nodal constraints $|u_h'(x_i)|^2 = 1$, $i = 0, 1, \dots, N$. The term $(\varepsilon^{-1}\|\mathcal{I}_{1,h}(|u_h|_D - 1)_+\|_{L^2}^2)^{1/3}$ is bounded by the third root of the potential part of the discrete energy. □

Remark 5 A stronger estimate on the constraint violation can be derived if the solution u and the Lagrange multiplier λ are sufficiently regular, so that the Euler–Lagrange equations hold in strong form, i.e., $\kappa u^{(4)} + \varepsilon^{-1}\nabla V_D(u) = (\lambda u')'$, which implies $\|\nabla V_D(u)\|_{L^\infty(I)} = \mathcal{O}(\varepsilon)$, where $|\nabla V_D(y)|$ is proportional to the distance of a point $y \in \mathbb{R}^3$ to the set D.

Our third convergence result follows from the unconditional energy stability of the numerical scheme and states that the sequence of corrections $(d_t u_h^k)_{k=1,2,\dots}$ converges to zero as $k \to \infty$. Moreover, it provides a bound on the violation of the arclength constraint due to its linearized treatment.

Proposition 6 *Given an inner product $(\cdot,\cdot)_\star$ on $H^2(I;\mathbb{R}^3)$, the iterates $(u_h^k)_{k=0,1,\dots}$ of scheme (6) satisfy*

$$E_{h,\varepsilon}\big[u_h^K\big] + \tau\sum_{k=1}^{K}\big\|d_t u_h^{k+1}\big\|_\star^2 \le E_{h,\varepsilon}\big[u_h^0\big]$$

for all $K \ge 0$, and, provided that $\|v\|_{L^\infty(I)} \le c_\star\|v\|_\star$ for all $v \in H^2(I;\mathbb{R}^3)$ with $L_{\mathrm{bc}}(v) = 0$,

$$\big\|\mathcal{I}_{1,h}\big|u_h'\big|^2 - 1\big\|_{L^\infty(I)} \le c_\star^2\tau E_{h,\varepsilon}\big[u_h^0\big].$$

Proof By the concavity of V_D^{cv} we have that

$$V_D^{\mathrm{cv}}\big(u_h^k\big) + \nabla V_D^{\mathrm{cv}}\big(u_h^k\big)\cdot\big(u_h^{k+1} - u_h^k\big) \ge V_D^{\mathrm{cv}}\big(u_h^{k+1}\big).$$

This implies that by choosing $v_h = d_t u_h^{k+1}$ in (6) we have

$$\big\|d_t u_h^{k+1}\big\|_\star^2 + d_t\left\{\frac{1}{2}\big\|\big[u_h^{k+1}\big]''\big\|^2 + \frac{1}{2\varepsilon}\int_I \mathcal{I}_h V_D\big(u_h^{k+1}\big)\,\mathrm{d}x\right\} \le 0.$$

Multiplication by τ and summation over $k = 0, 1, \dots, K-1$ yield the stability estimate. The orthogonality $[u_h^{k-1}]' \cdot [d_t u_h^k]'$ for $k = 1, 2, \dots, K$ at the nodes leads to the relation

$$\big|\big[u_h^k\big]'\big|^2 = \big|\big[u_h^{k-1}\big]'\big|^2 + \tau^2\big|\big[d_t u_h^k\big]'\big|^2.$$

Summing this identity over $k = 1, 2, \dots, K$, noting that $|[u_h^0]'|^2 = 1$ at the nodes, and including the energy stability prove the estimate. □

3 Elasticae in balls and cylinders

Our numerical calculations are performed in MATLAB and with the KNOTEVOLVE web application [9]. We consider closed elastic rods confined to balls and cylinders. The highly symmetric stationary configurations found for balls give rise to the following definition, which provides a concise classification via two integer numbers. For the scalar product $(d_t u_h^{k+1}, v_h)_\star$, we use the L^2 inner product. In this case the factor $c_\star$ is h-dependent with $c_\star \le ch^{-1/2}$ so that the step-size condition $\tau h^{-1/2} \to 0$ needs to be imposed to guarantee the results of the previous section. The parameter values $\kappa = 10$ and $\varepsilon = 1/(10\kappa)$ are employed if not stated otherwise.

Definition 7 An arclength parameterized curve is called a *μ-circle* if it is a μ-fold covered planar circle. It is called a *μ-ν-clew* if it shows a ν-fold symmetry around one axis running through the center of the ball. The integer μ is then defined as the winding number of u around the rotational axis.

3.1 Confined trefoil knot

As an illustrative example of the gradient flow, we use a trefoil knot of length 31.9 that is confined to a ball of radius 4.6 with $h \approx 0.3$ and $\tau = 0.1h$.[1] Snapshots of the evolution are depicted in Fig. 1. Also, the bending energy $\kappa\|[u_h^k]''\|^2/2$, the confinement energy $(2\varepsilon)^{-1}E_D[u_h^k]$, and the violation of arc-length parameterization $\|\mathcal{I}_{1,h}\{|[u_h^k]'|^2 - 1\}\|_{L^\infty}$ are visualized as functions of k.

First, the trefoil knot evolves into a double-covered circle. At some point, it unfolds into a bent lemniscate whose outermost points reach the surface of the ball. This configuration then moves to the left and starts to unfold into a buckled circle that runs close to the ball's surface. The final elastica is a 1-2-clew. The symmetry axis of the elastica, which is also depicted in Fig. 1, is different from the symmetry axis of the initial curve. The local curvature of the 1-2-clew is periodic along the curve with periodicity 4. We generally observe that the curvature of a μ-ν-clew is 2ν-periodic.

A similar shape was previously also obtained for modeling semiflexible biopolymers in spherical domains that are slightly smaller than the flat circle of the same length; see [40]. The shape that we call 1-2-clew also arises when packing a thick rope of maximal length without self-penetration on the sphere [28].

3.2 Closed curves in spheres

When confining a rod of length L to balls of varying radii, we observe a multitude of equilibrium configurations. Examples are illustrated in Fig. 2, where we used C_4 and C_5 symmetric initial configurations. Both the symmetry number ν and the winding number μ depend on the symmetry of the initial configuration and on the ratio L/R. All elasticae run close to the surface of the ball and slightly exceed the confining domain. With decreasing

[1] The example can be run via aam.uni-freiburg.de/knotevolve/torus-2-3-97?Rho=0&CnfmType=ellipsoid&CnfmRadius=4.6,4.6,4.6&tmax=30000&StepW=0.1

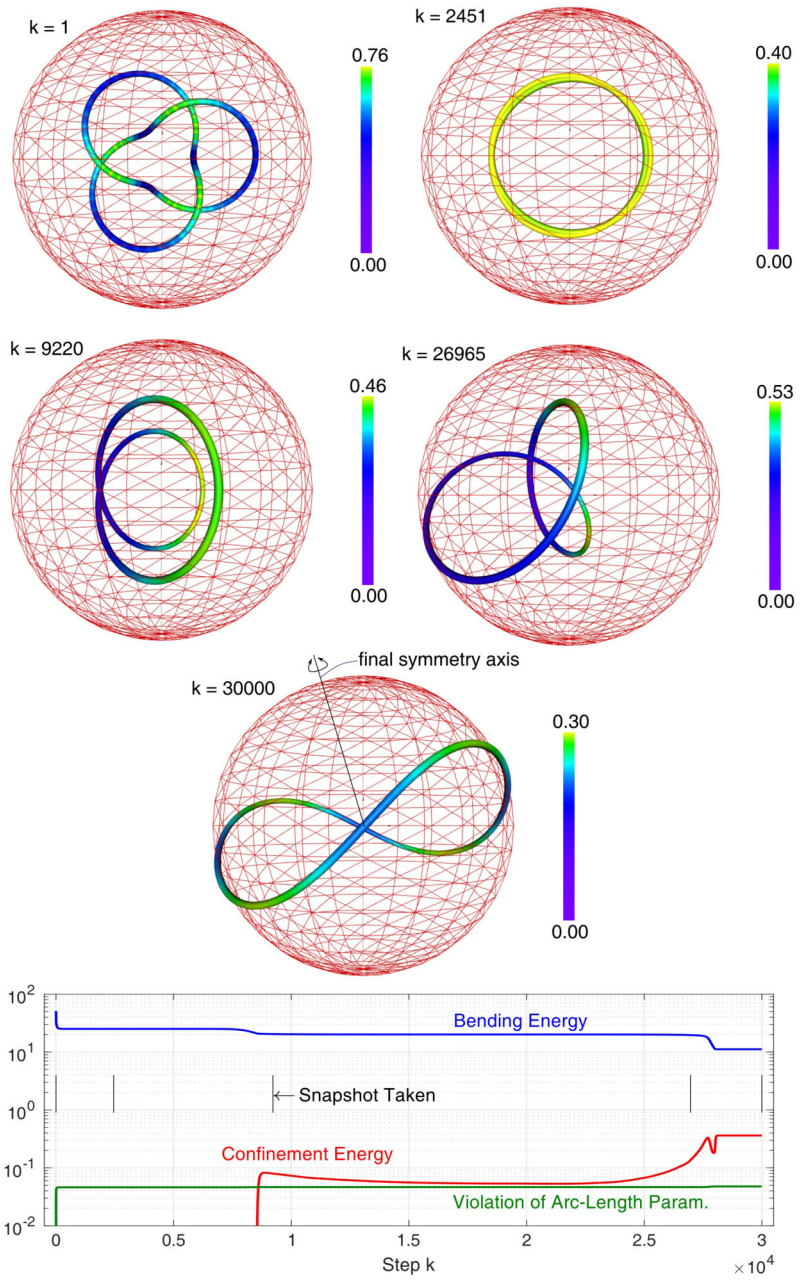

Figure 1 Evolution of a closed elastic curve in a ball of radius $R = 4.6$ to a 1-2-clew. The number k indicates the time steps, the color scheme represents the local curvature. Confinement energy and violation of arc-length parameterization are shown in the lower right panel

radius, either the winding number or the symmetry number is gradually increased by 2. This follows from an increasing number of self-intersections of the rod that always affect two of its segments. The gradient flow used to minimize the energy preserves certain symmetries. When starting with an even symmetry, the elastica is an odd-even-clew or an odd-circle as illustrated in Fig. 2. An initially odd rotational symmetry in turn generally leads to even-odd-clews or even-circles. An exception is the transition from the 2-1-clew

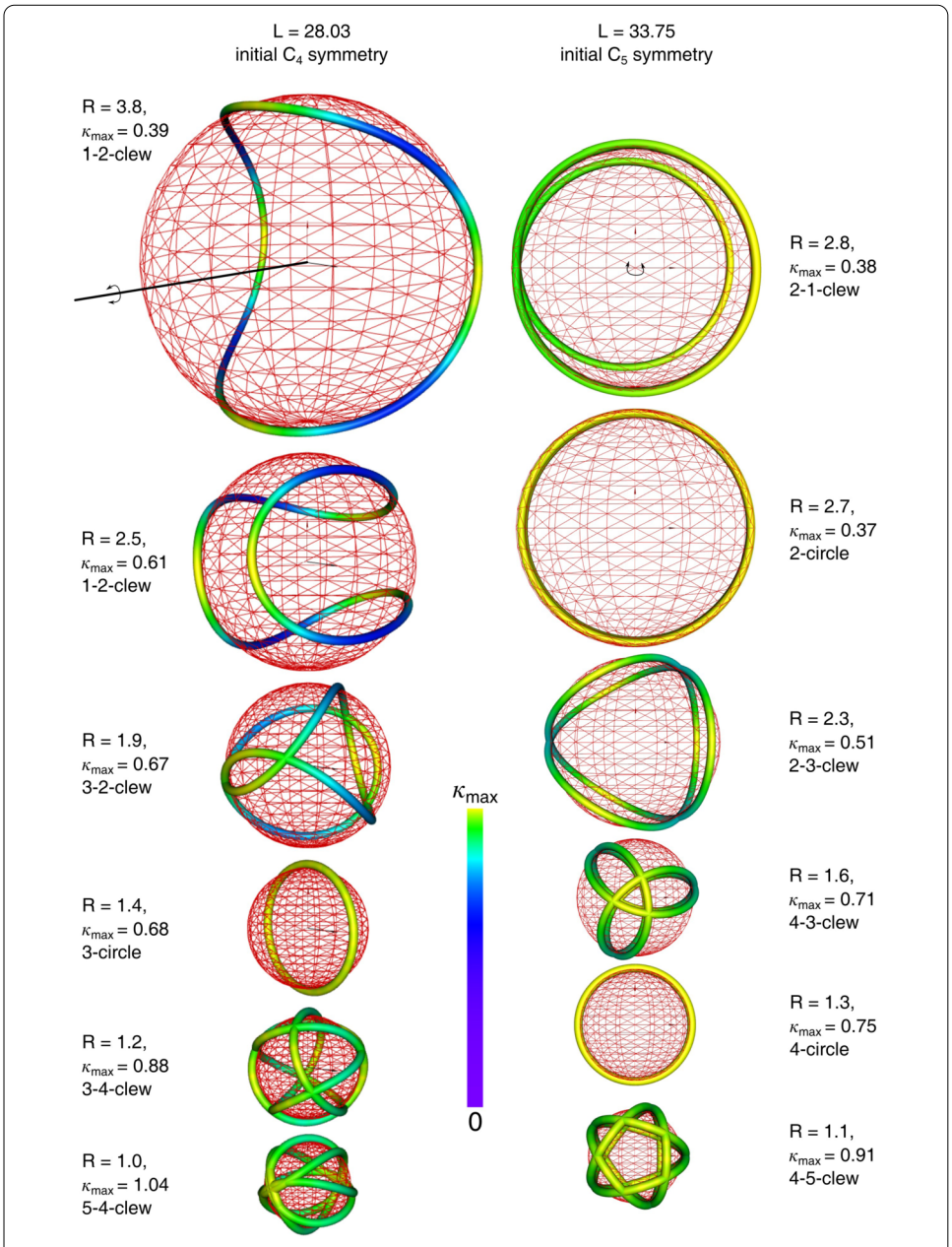

Figure 2 Elastica shapes obtained for two different initial configurations (left and right columns) and varying radii *R*. The color of the rod indicates the local curvature. The symmetry axis of the left column is indicated for the top configuration. In the right column, symmetry and view axes coincide

to the 1-2-clew as illustrated in the introductory example. This transition involves large deformations. When the radius of the ball is too small, the confinement is too restrictive for the curve to undergo such large transitions.

The parameter ε can be understood as a length scale of maximal penetration into the complement of D. Numerical experiments for an initial C_4 symmetric closed rod of length 28.38 confined to a sphere of radius 3.1 and for an initially C_5 symmetric closed rod of

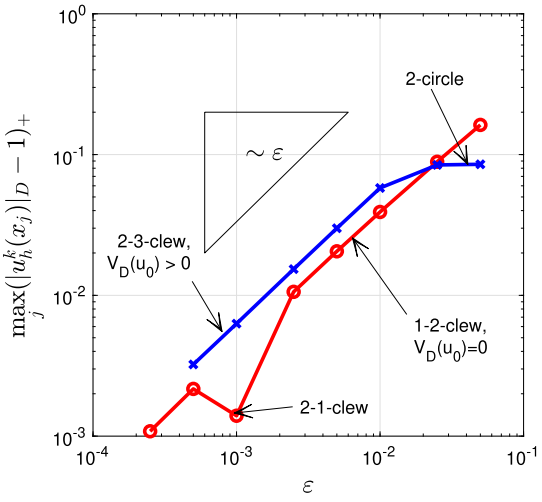

Figure 3 Maximal nodal penetration outside the confinement domain depending on ε

length 34.08 confined to a sphere of radius 2.5 were carried out for multiple values of ε.[2] The numerical results shown in Fig. 3 indicate that

$$\max_{j=0,\dots,N} \left(\left|u_h^k(x_j)\right|_D - 1\right)_+ = \mathcal{O}(\varepsilon).$$

Thus the maximal penetration decreases linearly with ε whilst not depending on whether the initial rod configuration lies inside D. This indicates that the estimate as sketched in Remark 5 is valid in the case of spherical confinements.

We can observe that when varying ε for the same initial configuration, the final shape is not unique; see Fig. 3. In the first example (dots), mainly 1-2-clews were obtained as final shapes, but for one value of ε, also a 2-1-clew could be observed. The second example (crosses), which relaxed to a 2-3-clew for sufficiently small ε, turned into a twofold covered circle whenever the confinement was too weak. This observation underlines that the energy landscape is nontrivially dependent on all parameters. A priori, it is in general difficult to specify which stationary configuration will be selected or if a given state is globally optimal.

The unconfined elastica of a closed rod of length L is the circle of radius $r_L = L/(2\pi)$. The bending energy of this elastica is given by $E_L = \kappa L/(2r_L^2) = 2\kappa\pi^2/L$. To categorize the equilibrium configurations of closed rods that are confined to balls of radius R, we evaluate $(E_{\text{bend}}/E_L)^{1/2}$ as a function of r_L/R. The first quantity measures the excess bending induced by the confinement, whereas the second quantity determines how many times too small the confining ball is compared to the unconfined elastica. We remark that for μ-fold covered circles, both quantities equal μ.

[2] In KNOTEVOLVE, these configurations can be loaded as torus knots with 101 nodes, $p = 1$, and either $q = 4$ or $q = 5$, respectively.

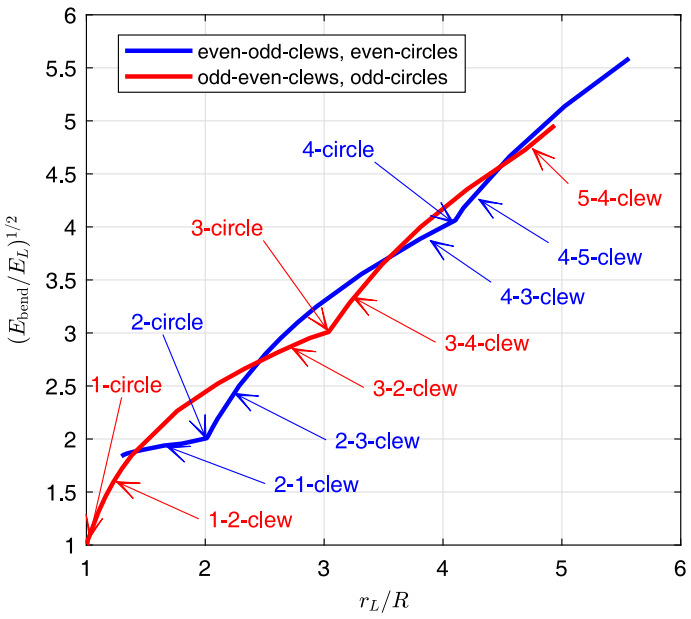

Figure 4 Normalized square root of the bending energy depending on the ratio r_L/R for the two observed elastica families

When starting with the four- and five-fold symmetric initial configurations, we observe two distinct families of the bending energy dependency on the ratio r_L/R. The result is shown in Fig. 4. The elasticae in the five-fold symmetric case follow the pattern 1-circle, 1-2-clew, 3-2-clew, 3-circle, 3-4-clew, 5-4-clew, etc. for increasing r_L/R. In the four-fold symmetric case, we find (1-circle, 1-2-clew), 2-1-clew, 2-circle, 2-3-clew, 4-3-clew, 4-circle, 4-5-clew, and so on. The first two are special as they involve a large deformation of the rod when transiting from the even-odd to odd-even. Both patterns are very regular and are expected to continue for larger r_L/R.

During the unfolding process, intermediate nearly stationary configurations are observed. These include a shape that could be called a 1-3-clew or multiply covered circles that are completely inside the ball. This can be seen in Fig. 1: The initial rod evolves into a two-fold covered circle in the first place; later, the circle opens up. These configurations seem to be saddle-point structures as they are attractive with respect to the previous configuration, whereas there are adjacent configurations with smaller total energy. As the numerical representation of the rod cannot match those saddle-points perfectly, the rod exits those configurations after a certain number of steps.

For irregularly shaped initial rod configurations, the previously described elastica shapes are found as well.[3] Hence the symmetry of the final shape can solely be attributed to the ratio r_L/R and to the question whether the initial configuration prefers the odd-even or even-odd elasticae family.

[3]See, for instance, a knot with crossing number 10 relaxing into a 3-2-clew: aam.uni-freiburg.de/knotevolve/10_053?Rho=0&StepW=0.1&CnfmType=ellipsoid&CnfmRadius=3,3,3

Conjecture 8 *Consider a rod of length L confined to a ball of radius R. Let* $r_L = L/(2\pi)$ *be the radius of the unconfined elastica, and let* $j \in \mathbf{N}$ *be a positive integer with* $j < r_L/R < j+1$. *Then there is a number* $\xi(j) \in (0,1)$ *such that the globally least bent confined elastica is a* j*-*$(j+1)$*-clew if* $r_L/R < j + \xi$. *Otherwise, the global optimizer is the* $(j+1)$*-*j*-clew. If* $r_L/R < 1$, *then the flat* 1*-circle is an exactly confined elastica. In the cases where* $r_L/R = j$, *the j-fold covered circle is the global elastica*.

Interestingly, all elasticae for $r_L/R \geq 1$ lie on the surface of the ball up to the penetration due to the finite potential. Brunnett and Crouch [17] derived a differential equation for the geodesic curvature κ_g of the rod on the sphere, i.e., the projection of the total curvature on the tangent plane at each point:

$$\kappa_g'' + \frac{1}{2}\kappa_g^3 + C\kappa_g = 0.$$

Here C is a constant consisting of the tension energy of the rod and the sphere square curvature. This differential equation can be solved by the Jacobi elliptic cosine function. The parameters of these functions must be adjusted so that the curvature is periodic. When using the solution to calculate the actual rod position, a nine-component ODE is solved, again imposing periodicity. This raises the question whether the resulting configurations coincide with our experimentally observed μ-ν-clews and μ-circles, thus leading to an analytic definition of our clews. For the μ-ν-clew, ν and μ should arise when taking the periodic boundary conditions into account for the geodesic curvature and the rod position, respectively. It is also of analytic interest if all elasticae confined to balls are in fact elasticae on the sphere. A proof would however go beyond the scope of this paper.

3.3 Closed curves in cylinders

We close our discussion by experimentally investigating closed curves confined to cylinders of different heights and radii.[4] As shown in Fig. 5, large cylinder heights apparently lead to flat configurations that resemble semicircles connected by straight lines. If the cylinder is long enough, then we assume that the true global elastica consists of two semicircles connected by two straight lines. If the height and diameter are equal, then we observe a shape similar to a 4-3-clew (for height and diameter 6) or a 3-2-clew (for height and diameter 8). Other combinations of height and diameter reveal a large variety of optimal shapes. A concise classification as in the case of spherical confinement however is not obvious.

4 Conclusions

We have devised a stable and convergent numerical scheme for approximation of confined inextensible curves with low bending energy. The scheme leads to an experimental classification of stationary configurations. Numerical studies confirm the theoretical results.

[4]See, for instance, aam.uni-freiburg.de/knotevolve/torus-1-13-100?Rho=0&StepW=0.2&CnfmType=cylinder-z&CnfmRadius=3,3,3&tmax=200000

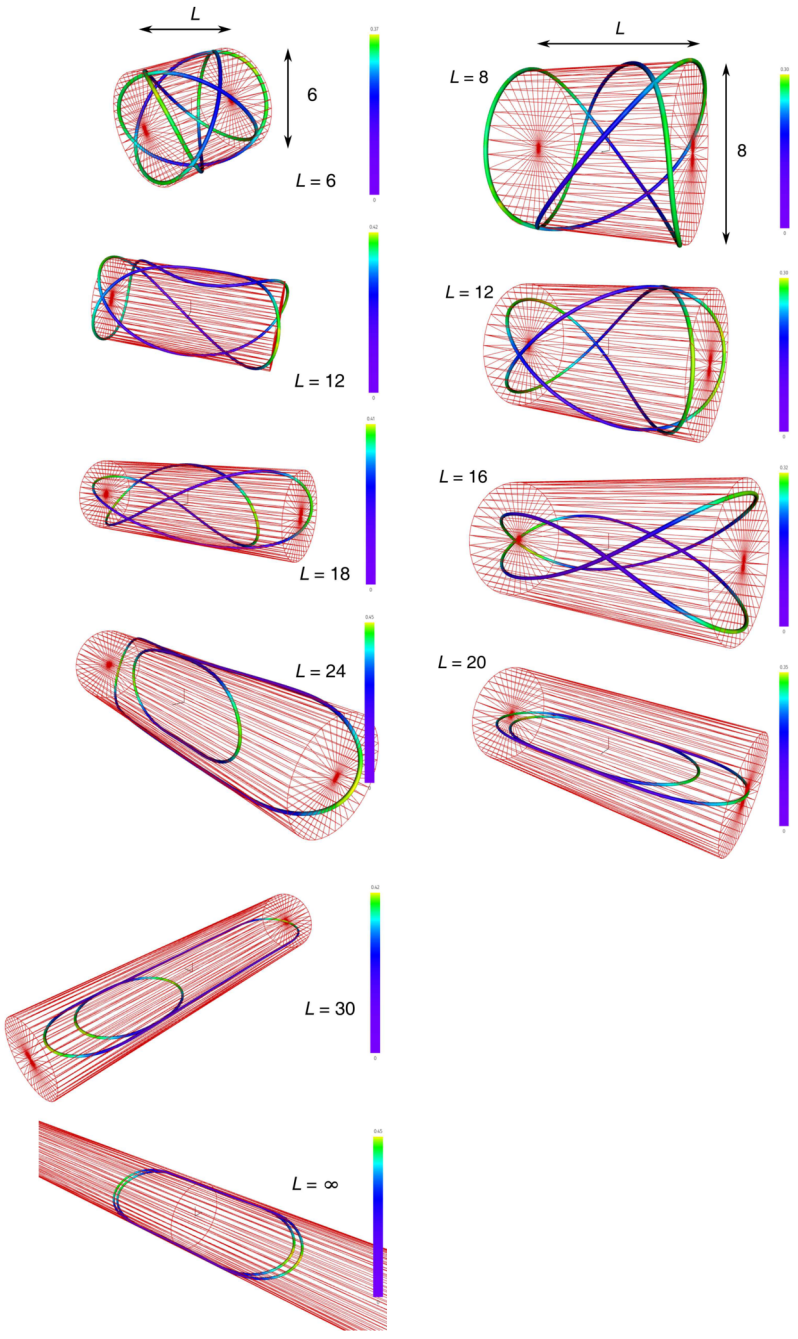

Figure 5 Stationary closed curves in cylindrical domains with radii $R = 3$ (left) and $R = 4$ (right) and different heights (increasing from top to bottom)

Acknowledgements
Not applicable.

Funding
Open Access funding enabled and organized by Projekt DEAL.

Availability of data and materials
Not applicable.

Declarations

Competing interests
The authors declare no competing interests.

Author contribution
All results have been obtained in joint work. All authors read and approved the final manuscript.

Publisher's Note

Springer Nature remains neutral with regard to jurisdictional claims in published maps and institutional affiliations.

Received: 25 April 2022 Accepted: 10 October 2022 Published online: 21 October 2022

References

1. Balaeff, A., Mahadevan, L., Schulten, K.: Modeling DNA loops using the theory of elasticity. Phys. Rev. E **73**, 031919 (2006). https://doi.org/10.1103/PhysRevE.73.031919
2. Barrett, J.W., Garcke, H., Nürnberg, R.: Numerical approximation of anisotropic geometric evolution equations in the plane. IMA J. Numer. Anal. **28**(2), 292–330 (2008). https://doi.org/10.1093/imanum/drm013
3. Barrett, J.W., Garcke, H., Nürnberg, R.: Numerical approximation of gradient flows for closed curves in $\mathbb{R}^d$. IMA J. Numer. Anal. **30**(1), 4–60 (2010). https://doi.org/10.1093/imanum/drp005
4. Barrett, J.W., Garcke, H., Nürnberg, R.: The approximation of planar curve evolutions by stable fully implicit finite element schemes that equidistribute. Numer. Methods Partial Differ. Equ. **27**(1), 1–30 (2011). https://doi.org/10.1002/num.20637
5. Barrett, J.W., Garcke, H., Nürnberg, R.: Finite element methods for fourth order axisymmetric geometric evolution equations. J. Comput. Phys. **376**, 733–766 (2019). https://doi.org/10.1016/j.jcp.2018.10.006
6. Barrett, J.W., Garcke, H., Nürnberg, R.: Stable discretizations of elastic flow in Riemannian manifolds. SIAM J. Numer. Anal. **57**(4), 1987–2018 (2019). https://doi.org/10.1137/18M1227111
7. Bartels, S.: A simple scheme for the approximation of the elastic flow of inextensible curves. IMA J. Numer. Anal. **33**(4), 1115–1125 (2013). https://doi.org/10.1093/imanum/drs041
8. Bartels, S.: Finite element simulation of nonlinear bending models for thin elastic rods and plates. In: Geometric Partial Differential Equations. Part I. Handb. Numer. Anal., vol. 21, pp. 221–273. Elsevier/North-Holland, Amsterdam (2020)
9. Bartels, S., Falk, P., Weyer, P.: KNOTEVOLVE – a tool for relaxing knots and inextensible curves (2020). https://aam.uni-freiburg.de/knotevolve/
10. Bartels, S., Palus, C.: Stable gradient flow discretizations for simulating bilayer plate bending with isometry and obstacle constraints. IMA J. Numer. Anal. **42**, 1903–1928 (2022). https://doi.org/10.1093/imanum/drab050
11. Bartels, S., Reiter, P.: Numerical solution of a bending-torsion model for elastic rods. Numer. Math. **146**(4), 661–697 (2020). https://doi.org/10.1007/s00211-020-01156-6
12. Bartels, S., Reiter, P.: Stability of a simple scheme for the approximation of elastic knots and self-avoiding inextensible curves. Math. Comput. **90**(330), 1499–1526 (2021). https://doi.org/10.1090/mcom/3633
13. Bartels, S., Reiter, P., Riege, J.: A simple scheme for the approximation of self-avoiding inextensible curves. IMA J. Numer. Anal. **38**(2), 543–565 (2018). https://doi.org/10.1093/imanum/drx021
14. Bonito, A., Guignard, D., Nochetto, R., Yang, S.: Numerical analysis of the LDG method for large deformations of prestrained plates (2021). arXiv:2106.13877
15. Bonito, A., Guignard, D., Nochetto, R.H., Yang, S.: LDG approximation of large deformations of prestrained plates. J. Comput. Phys. **448**, 110719 (2022). https://doi.org/10.1016/j.jcp.2021.110719
16. Boué, L., Adda-Bedia, M., Boudaoud, A., Cassani, D., Couder, Y., Eddi, A., Trejo, M.: Spiral patterns in the packing of flexible structures. Phys. Rev. Lett. **97**, 166104 (2006). https://doi.org/10.1103/PhysRevLett.97.166104
17. Brunnett, G., Crouch, P.E.: Elastic curves on the sphere. Adv. Comput. Math. **2**(1), 23–40 (1994). https://doi.org/10.1007/BF02519034
18. Choi, M.C., Santangelo, C.D., Pelletier, O., Kim, J.H., Kwon, S.Y., Wen, Z., Li, Y., Pincus, P.A., Safinya, C.R., Kim, M.W.: Direct observation of biaxial confinement of a semiflexible filament in a channel. Macromolecules **38**(23), 9882–9884 (2005). https://doi.org/10.1021/ma051348n
19. Dall'Acqua, A., Lin, C.-C., Pozzi, P.: Evolution of open elastic curves in $\mathbb{R}^n$ subject to fixed length and natural boundary conditions. Analysis **34**(2), 209–222 (2014). https://doi.org/10.1515/anly-2014-1249
20. Deckelnick, K., Dziuk, G.: Error analysis for the elastic flow of parametrized curves. Math. Comput. **78**(266), 645–671 (2009). https://doi.org/10.1090/S0025-5718-08-02176-5
21. Deckelnick, K., Dziuk, G., Elliott, C.M.: Computation of geometric partial differential equations and mean curvature flow. Acta Numer. **14**, 139–232 (2005). https://doi.org/10.1017/S0962492904000224
22. Dill, E.H.: Kirchhoff's theory of rods. Arch. Hist. Exact Sci. **44**(1), 1–23 (1992). https://doi.org/10.1007/BF00379680
23. Donato, C.C., Gomes, M.A.F., de Souza, R.E.: Scaling properties in the packing of crumpled wires. Phys. Rev. E **67**, 026110 (2003). https://doi.org/10.1103/PhysRevE.67.026110
24. Dondl, P.W., Mugnai, L., Röger, M.: Confined elastic curves. SIAM J. Appl. Math. **71**(6), 2205–2226 (2011). https://doi.org/10.1137/100805339
25. Dörfler, W., Nürnberg, R.: Discrete gradient flows for general curvature energies. SIAM J. Sci. Comput. **41**(3), A2012–A2036 (2019). https://doi.org/10.1137/18M122844X
26. Dziuk, G., Kuwert, E., Schätzle, R.: Evolution of elastic curves in $\mathbb{R}^n$: existence and computation. SIAM J. Math. Anal. **33**(5), 1228–1245 (2002). https://doi.org/10.1137/S0036141001383709
27. Furrer, P.B., Manning, R.S., Maddocks, J.H.: DNA rings with multiple energy minima. Biophys. J. **79**(1), 116–136 (2000). https://doi.org/10.1016/S0006-3495(00)76277-1
28. Gerlach, H., von der Mosel, H.: What are the longest ropes on the unit sphere? Arch. Ration. Mech. Anal. **201**(1), 303–342 (2011). https://doi.org/10.1007/s00205-010-0390-y

29. Green, A.E., Laws, N., Naghdi, P.M.: A linear theory of straight elastic rods. Arch. Ration. Mech. Anal. **25**(4), 285–298 (1967). https://doi.org/10.1007/BF00250931
30. Grothaus, M., Marheineke, N.: On a nonlinear partial differential algebraic system arising in the technical textile industry: analysis and numerics. IMA J. Numer. Anal. **36**(4), 1783–1803 (2016). https://doi.org/10.1093/imanum/drv056
31. Hornung, P.: Deformation of framed curves with boundary conditions. Calc. Var. Partial Differ. Equ. **60**(3), Paper No. 87 (2021). https://doi.org/10.1007/s00526-021-01980-0
32. Kirchhoff, G.: Ueber das Gleichgewicht und die Bewegung eines unendlich dünnen elastischen Stabes. J. Reine Angew. Math. **56**, 285–313 (1859). https://doi.org/10.1515/crll.1859.56.285
33. Langer, J., Singer, D.A.: Knotted elastic curves in $\mathbb{R}^3$. J. Lond. Math. Soc. (2) **30**(3), 512–520 (1984). https://doi.org/10.1112/jlms/s2-30.3.512
34. Langer, J., Singer, D.A.: Curve straightening and a minimax argument for closed elastic curves. Topology **24**(1), 75–88 (1985). https://doi.org/10.1016/0040-9383(85)90046-1
35. Leoni, G.: A First Course in Sobolev Spaces, 2nd edn. Graduate Studies in Mathematics, vol. 181, p. xxii+734. Am. Math. Soc., Providence (2017). https://doi.org/10.1090/gsm/181
36. Manhart, A., Oelz, D., Schmeiser, C., Sfakianakis, N.: An extended filament based lamellipodium model produces various moving cell shapes in the presence of chemotactic signals. J. Theor. Biol. **382**, 244–258 (2015). https://doi.org/10.1016/j.jtbi.2015.06.044
37. Mora, M.G., Müller, S.: Derivation of the nonlinear bending-torsion theory for inextensible rods by Γ-convergence. Calc. Var. Partial Differ. Equ. **18**(3), 287–305 (2003). https://doi.org/10.1007/s00526-003-0204-2
38. Mulcahy, C.G., Su, T., Wicks, N., Reis, P.M.: Extending the reach of a rod injected into a cylinder through axial rotation. J. Appl. Mech. **83**(5), 051003 (2016). https://doi.org/10.1115/1.4032500
39. Öelz, D.B.: On the curve straightening flow of inextensible, open, planar curves. SeMA J. **54**, 5–24 (2011). https://doi.org/10.1007/bf03322585
40. Ostermeir, K., Alim, K., Frey, E.: Buckling of stiff polymer rings in weak spherical confinement. Phys. Rev. E **81**, 061802 (2010). https://doi.org/10.1103/PhysRevE.81.061802
41. Ranner, T.: A stable finite element method for low inertia undulatory locomotion in three dimensions. Appl. Numer. Math. **156**, 422–445 (2020). https://doi.org/10.1016/j.apnum.2020.05.009
42. Reiter, P., Schumacher, H.: Sobolev gradients for the Möbius energy. Arch. Ration. Mech. Anal. **242**(2), 701–746 (2021). https://doi.org/10.1007/s00205-021-01680-1
43. Shi, Y., Hearst, J.E.: The Kirchhoff elastic rod, the nonlinear Schrödinger equation, and DNA supercoiling. J. Chem. Phys. **101**(6), 5186–5200 (1994). https://doi.org/10.1063/1.468506
44. Walker, S.: A descent scheme for thick elastic curves with self-contact and container constraints. Preprint (2021). https://www.math.lsu.edu/~walker/pdfs/Walker2021_elastic_curve_self_contact.pdf
45. Walker, S.W.: Shape optimization of self-avoiding curves. J. Comput. Phys. **311**, 275–298 (2016). https://doi.org/10.1016/j.jcp.2016.02.011
46. Wojtowytsch, S.: Confined elasticae and the buckling of cylindrical shells. Adv. Calc. Var. **14**(4), 555–587 (2021). https://doi.org/10.1515/acv-2019-0033

Submit your manuscript to a SpringerOpen journal and benefit from:

- ► Convenient online submission
- ► Rigorous peer review
- ► Open access: articles freely available online
- ► High visibility within the field
- ► Retaining the copyright to your article

Submit your next manuscript at ► springeropen.com